Anatase TiO_2 single crystals with a large percentage of reactive {001} facets

Hua Gui Yang[1*], Cheng Hua Sun[1,2*], Shi Zhang Qiao[1], Jin Zou[3], Gang Liu[1,4], Sean Campbell Smith[1,2], Hui Ming Cheng[4] & Gao Qing Lu[1]

[1] *ARC Centre of Excellence for Functional Nanomaterials, School of Engineering and Australian Institute for Bioengineering and Nanotechnology, The University of Queensland, QLD 4072, Australia*
[2] *Centre for Computational Molecular Science, Australian Institute for Bioengineering and Nanotechnology, The University of Queensland, QLD 4072, Australia*
[3] *Centre for Microscopy and Microanalysis and School of Engineering, The University of Queensland, QLD 4072, Australia*
[4] *Shenyang National Laboratory for Materials Science, Institute of Metal Research, Chinese Academy of Sciences, 72 Wenhua Road, Shenyang 110016, China*

**These authors contributed equally to this work.*

Due to their scientific and technological importance, inorganic single crystals with highly reactive surfaces have long been targeted[1-13]. Unfortunately, surfaces with high reactivity usually diminish rapidly during the crystal growth process as a result of the minimization of surface energy. A typical example is titanium dioxide (TiO_2), which has promising energy and environmental applications [14-17]. Most available anatase TiO_2 crystals are mainly dominated by the thermodynamically stable {101} facets (more than 94% according to Wulff construction[10]), as opposed to the much more reactive {001} facets.[8-13, 18-20]. Here, we demonstrate that for fluorine-terminated surfaces this relative stability is reversed - {001} is energetically preferable to {101}. We explored this effect systematically for a range of non-metallic atoms (H, B, C, N, O, F, Si, P, S, Cl, Br, I) by first-principle quantum chemical calculations. Based on theoretical predictions, we have synthesized uniform anatase TiO_2 single crystals with a high percentage (47%) of {001} facets by using hydrofluoric acid (HF) as a morphology controlling agent. Moreover, the fluorated surface of anatase single crystals can be easily cleaned to render a fluorine-free surface by heat treatment without altering the crystal structure and morphology.

The surface stability and reactivity of inorganic single crystals (SCs) have long been thought to be dominated by their surface chemistry, whose effect on the equilibrium morphology is critical for the synthesis of SCs with high reactivity[1-13, 21]. For anatase TiO_2, both theoretical and experimental studies found that the minority {001} facets in the equilibrium state are especially reactive[8]. However, large high-quality anatase SCs with a high percentage of {001} facets have not been realized[22-24]. An early study[23] showed that the hydrothermal treatment of hydrous titanium (IV) oxide in the presence of HF resulted in irregular aggregates of polymorphic TiO_2 with anhedral

morphology. Recently, anatase SCs were synthesized by chemical transport reactions, but such process suffered from long reaction time, low-purity and no {001} facets[24]. Therefore, preparation of uniform and high-purity anatase SCs with controllable crystallographic facets still remains a great challenge.

To this end, various adsorbate atoms have been attempted to change the relative stabilities of different crystal facets[19-23]. For anatase TiO_2, among oxygenated surfaces, {100} is the most stable, rather than {101}, in clean and hydrogenated conditions[5,10,21]. However, both H- and O-terminated anatase surfaces present high surface energies (γ), which restrict the formation of large single-crystal anatase. High values of γ are mainly attributed to the high bonding energies (D_0) of H-H (436.0 kJ/mol) and O-O (498.4 kJ/mol)[25]. Therefore, to find a low D_0 element with high bonding to Ti could be an effective solution for stabilizing the faceted surfaces. Interestingly, F is such an element as $D_0^{F\text{-}F}$ = 158.8 kJ/mol[25] and $D_0^{F\text{-}Ti}$ = 569.0 kJ/mol[26]. To further explore the effects of various adsorbate atoms, we carried out a systematic investigation of 12 non-metallic atoms X (X = H, B, C, N, O, F, Si, P, S, Cl, Br, I) using first-principle calculations. Fig. 1a-d depicts the models of clean and X-terminated surfaces of (001) and (101). The calculated γ values for different adsorbates are illustrated in Fig. 1e, from which two conclusions can be drawn: (i) among the 12 non-metal-terminated surfaces and the clean surfaces, F-terminated anatase surfaces have the lowest γ for both (001) and (101); and (ii) for F-terminated anatase surfaces, (001) is more stable than (101). These results indicate that a high percentage of anatase {001} facets may be achievable if their surface is surrounded by F. Furthermore, based on the shape dependent thermodynamic model proposed by Barnard et al[27], the optimized ratio of B/A (as denoted in the inset of Fig. 1) and the percentage of {001} facets can be predicted if γ is known. As shown in Fig. 1f, the F-terminated surfaces have the

highest degree of truncation (approximately B/A→1) and, in turn, the F-terminated surfaces of anatase TiO_2 should be dominated by {001} facets.

To verify these theoretical predictions, titanium tetrafluoride (TiF_4) aqueous solution and HF were used as the anatase SCs precursor and crystallographic controlling agent, respectively, to generate the truncated anatase bipyramids. Representative scanning electron microscopy (SEM) images of the products synthesized with different concentrations of TiF_4 and reaction times are shown in Fig. 2a and 2d. Based on the symmetries of anatase TiO_2, the two flat squared surfaces must be {001} facets while the other eight isosceles trapezoidal surfaces are {101} facets of anatase SCs (further proved in Fig. 3 and Fig. S7). The yield of anatase TiO_2 SCs is around 90%, even though some agglomerates and/or irregular particles (see Fig. S4) could be occasionally observed. To examine the uniformity of the synthesized anatase crystals, the length of A and the ratio of B/A were statistically analyzed and their results are presented in Figs. 2b, 2c, 2e, 2f, respectively. The average lengths are 1.66 μm and 1.64 μm with relative standard deviations (RSDs) of 8.4% and 15.8% (Figs. 2b and 2e) for the cases shown in Figs. 2a and 2d. Their degrees of truncation (assigned as B/A) are 0.77 and 0.84 with RSDs of 4.3% and 5.1% (Figs. 2c and 2f), respectively. The percentages of {001} facets can be estimated as 35% and 47%, respectively. The fact that anatase SCs exhibit a high degree of truncation generated under low concentration of TiF_4 may be attributed to the higher fluorine density on the surface thus making the isotropic growth more obvious. This is remarkably consistent with our theoretical predictions, and can be well understood from the viewpoints of shape-control chemistry[20, 21]. Previously, Lazzeri and Selloni found that the surface free energy of (001) can be reduced to 0.51 J/m^2 due to the (1×4) reconstruction[13], suggesting that such reconstruction can also stabilize (001). However, based on their

calculated values of γ, the optimized ratio of B/A is around 0.37, far from 0.77 and 0.84 obtained in our experiments, indicating that the high percentage of {001} facets is *not* resulted from such reconstruction. According to the detailed calculations based on a perfect (1×1) unit cell and (4×4) supercells of (001) (Supplementary Information Part I), all surfaces terminated by fluorine atoms present very low values of γ, so it is believed that the stabilization effect of fluorine atoms is the essential reason that the percentage of {001} facets can be as high as 47% in our experiments. Regarding the stabilization mechanism, a detailed analysis of the surface geometries has been carried out (see Supplementary Information Part I). Under clean conditions, the balance between the O-O repulsions and the attractive Ti-O π interactions is broken due to the cleavage of surfaces, thus causing unsaturated oxygen and titanium atoms to move outward (see Table S1). However, with the formation of Ti-F bonds, surface oxygen and titanium atoms move inward and outward dramatically due to the strong repulsive and attractive interactions of O-F and Ti-F, respectively. This analysis is consistent with the calculated electronic structures (see Fig. S3) because both Ti_{3d} and O_{2p} can interact with F_{2p} dramatically. Thereby, a new balance between O-O/F-O repulsions and Ti-O/Ti-F attractions can be established, which stabilizes Ti and O atoms on the surfaces. As a further confirmation, no crystal facet control was observed in the absence of HF and only hollow spherical polycrystalline anatase particles were formed (see Fig. S5)[28]. HF here is believed to possibly play dual roles: retarding hydrolysis of the titanium precursor and reducing surface energy to promote the isotropic growth along [010] and [100] [18,20], as illustrated in Fig.1a-f. Compared with the sample in Fig. 2a, the anatase SCs obtained in shorter reaction times show a smaller size and a higher degree of truncation than those in Fig. 2a (e.g., A = 850 nm and B/A = 0.84 at 8 h, depicted in Fig. S6). More importantly, according to the

theoretical predictions (Fig. 1f), the B/A value can be as high as 1.0 for the fully F-terminated surfaces; this important prediction indicates that ultrathin TiO_2 nanosheets may be synthesized.

Bright field images of transmission electron microscopy (TEM) and selected-area electron diffraction (SAED) patterns confirm that each free standing crystal shows single-crystalline characteristics, as depicted in Fig. 3a-b. The SAED patterns can be indexed into diffraction spots of the [001] zone[28]. The high resolution TEM image (Fig. 3c) shows the (200) and (020) atomic planes with a lattice spacing of 1.89 Å and 90^o interfacial angle[28]. A corresponding fast Fourier transform (FFT) filtered spot diagram of tetragonal atomic arrangement on the (001) surface is shown in Fig. 3d. Furthermore, the interfacial angle between two parallel faces and other surrounding faces is 68.3 ± 0.3^o on average (shown in Fig. S7); this value is identical to the theoretical value between the {001} and {101} facets of anatase[5].

X-ray diffraction (XRD) pattern is shown in Fig. 4a and all diffraction peaks match well with the crystal structure of the anatase TiO_2 phase (space group: $I4_1/amd$)[28]. X-ray photoelectron spectroscopy (XPS) spectrum of F 1s core electrons (Fig. 4b) for the anatase SCs clearly matches the model description in Fig. 1a-d; the measured binding energy (BE) is 684.5 eV only, which is a typical value for the fluorated TiO_2 system such as $TiOF_2$ or ≡Ti-F species on the TiO_2 crystal surface[29]. Furthermore, the oxidation state of the Ti element in the same materials (Ti $2p_{3/2}$, BE = 458.8 eV; Ti $2p_{1/2}$, BE = 464.3 eV) is identical to that of bulk TiO_2 as reported previously[30]. From the XPS results, we can conclude that the atomic incorporation or substitution of F for O in the anatase TiO_2 crystal lattice (doping process) can be safely ruled out. These results strongly support the initial theoretical predictions and our surface atomic model, that is, the high fluorine-titanium bonding energy lowers the surface energy of

the (001) dramatically thus making it more stable than (101) in our reaction media. Importantly, the fluorated surface of anatase SCs can be easily transformed to a clean fluorine-free surface through a heat treatment process at 600 ^{o}C for 90 min without changing its crystal structure and morphology (Fig. S8).

The well-defined high purity anatase SCs synthesized in this work would be very useful as model single crystals for fundamental studies in surface science. High purity anatase SCs with a high percentage of reactive {001} facets are promising for applications in solar cells, photonic and optoelectronic devices, sensors and photocatalysis. Furthermore, this study illustrates the power of combining first-principle calculations and experimental techniques to achieve engineering of surface and crystallographic characteristics of crystalline materials.

METHODS SUMMARY

Theoretical. Surface free energies were calculated using density functional theory within the generalized-gradient approximation. In each case, stoichiometric slab models (1×1) were employed, with all atoms being relaxed without any constraint.

Experimental. Titanium tetrafluoride (TiF_4) aqueous solution (varying between 2.67 and 5.33 mM) and hydrofluoric acid (HF, 10% w/w) were used as the precursor and the crystallographic controlling agent, respectively, to prepare anatase TiO_2 SCs. The reaction was carried out in a Teflon-lined autoclave at 180 ^{o}C for 2 to 20 h.

References

1. Tian, N., Zhou, Z. Y., Sun, S. G., Ding, Y. & Wang, Z. L. Synthesis of tetrahexahedral platinum nanocrystals with high-index facets and high electro-oxidation activity. *Science* **316**, 732-735 (2007).
2. Bikondoa, O., Pang, C. L., Ithnin, R., Muryn, C. A., Onishi, H. & Thornton, G. Direct visualization of defect-mediated dissociation of water on TiO_2 (110). *Nature Mater.* **5,** 189-192 (2006).
3. Dulub, O., Batzill, M., Solovev, S., Loginova, E., Alchagirov, A., Madey, T. E. & Diebold, U. Electron-induced oxygen desorption from the TiO_2 (011)-2x1 surface leads to self-organized vacancies. *Science* **317,** 1052-1056 (2007).
4. Gong, X. Q., Selloni, A., Batzill, M. & Diebold, U. Steps on anatase TiO_2 (101). *Nature Mater.* **5,** 665-670 (2006).
5. Diebold, U. The surface science of titanium dioxide. *Surf. Sci. Rep.* **48,** 53-229 (2003).
6. Thomas, A. G., Flavell, W. R., Kumarasinghe, A. R., Mallick, A. K., Tsoutsou, D. & Smith, G. C. Resonant photoemission of anatase TiO_2 (101) and (001) single crystals. *Phys. Rev. B* **67,** 035110 (2003).
7. Kavan, L., Grätzel, M., Gilbert, S. E., Klemenz, C. & Scheel, H. J. Electrochemical and photoelectrochemical investigation of single-crystal anatase. *J. Am. Chem. Soc.* **118,** 6716-6723 (1996).
8. Gong, X. Q. & Selloni, A. Reactivity of anatase TiO_2 nanoparticles: the role of the minority (001) surface. *J. Phys. Chem. B* **109,** 19560-19562 (2005).
9. Herman, G. S., Sievers, M. R. & Gao, Y. Structure determination of the two-domain (1 x 4) anatase TiO_2 (001) surface. *Phys. Rev. Lett.* **84,** 3354-3357 (2000).
10. Lazzeri, M., Vittadini, A. & Selloni, A. Structure and energetics of stoichiometric TiO_2 anatase surfaces. *Phys. Rev. B* **63,** 155409 (2001).
11. Vittadini, A., Selloni, A., Rotzinger, F. P. & Grätzel, M. Structure and energetics of water adsorbed at TiO_2 anatase (101) and (001) surfaces. *Phys. Rev. Lett.* **81,** 2954-2957 (1998).
12. Vittadini, A., Casarin, M. & Selloni, A. Chemistry *of* and *on* TiO_2-anatase surfaces by DFT calculations: a partial review. *Theor. Chem. Acc.* **117,** 663-671 (2007).

13. Lazzeri, M. & Selloni, A. Stress-driven reconstruction of an oxide surface: the anatase TiO_2 (001)-(1 x 4) surface. *Phys. Rev. Lett.* **87,** 266105 (2001).
14. Fujishima, A. & Honda, K. Electrochemical photolysis of water at a semiconductor electrode. *Nature* **238,** 37-38 (1972).
15. O'Regan, B. & Grätzel, M. A low-cost, high efficiency solar cell based on dye-sensitized colloidal TiO_2 films. *Nature* **353,** 737-740 (1991).
16. Grätzel, M. Photoelectrochemical cells. *Nature* **414,** 338-344 (2001).
17. Barbé, C. J., Arendse, F., Comte, P., Jirousek, M., Lenzmann, F., Shklover, V. & Grätzel, M. Nanocrystalline titanium oxide electrodes for photovoltaic applications. *J. Am. Ceram. Soc.* **80,** 3157-3171 (1997).
18. Penn, R. L. & Banfield, J. F. Morphology development and crystal in nanocrystalline aggregates under hydrothermal conditions: Insights from titania. *Geochimica et Cosmochimica Acta* **63,** 1549-1557 (1999).
19. Zaban, A., Aruna, S. T., Tirosh, S., Gregg, B. A. & Mastai, Y. The effect of the preparation condition of TiO_2 colloids on their surface structures. *J. Phys. Chem. B* **104**, 4130-4133 (2000).
20. Jun, Y. W., Casula, M. F., Sim, J.-H., Kim, S. Y., Cheon, J. & Alivisatos, A. P. Surfactant-assisted elimination of a high energy facet as a means of controlling the shapes of TiO_2 nanocrystals. *J. Am. Chem. Soc.* **125,** 15981-15985 (2003).
21. Barnard, A. S. & Curtiss, L. A. Prediction of TiO_2 nanoparticle phase and shape transitions controlled by surface chemistry. *Nano Lett.* **5,** 1261-1266 (2005).
22. Chen, X. & Mao, S. Titanium dioxide nanomaterials: synthesis, properties, modifications, and applications. *Chem. Rev.* **107**, 2891-2959 (2007)
23. Izumi, F. The polymorphic crystallization of titanium (IV) oxide under hydrothermal conditions. II. The roles of inorganic anions in the nucleation of rutile and anatase from acid solutions. *Bull. Chem. Soc. Jpn.* **51,** 1771-1776 (1978).
24. Berger, H., Tang, H. & Lévy, F. Growth and raman spectroscopic characterization of TiO_2 anatase single crystals. *J. Cryst. Growth* **130,** 108-112 (1993).

25. Zmbov, K. F. & Margrave, J. L. Mass spectrometric studies at high temperatures. XVI. Sublimation pressures for titanium (III) fluoride and the stabilities of TiF_2 (g) and TiF (g). *J. Phys. Chem.* **71**, 2893-2895 (1967)
26. Huber, K. P. & Herzberg, G. Molecular Spectra and Molecular Structure Constants of Diatomic Molecules. (Van Nostrand, New York, 1979).
27. Barnard, A. S. & Zapol, P. A model for the phase stability of arbitrary nanoparticles as a function of size and shape. *J. Chem. Phys.* **121**, 4276-4283 (2004).
28. Yang, H. G. & Zeng, H. C. Preparation of hollow anatase TiO_2 Nanospheres via Ostwald ripening. *J. Phys. Chem. B* **108**, 3492-3495 (2004).
29. Yu, J. C, Yu, J., Ho, W., Jiang, Z. & Zhang, L. Effects of F^- doping on the photocatalytic activity and microstructures of nanocrystalline TiO_2 powders. *Chem. Mater.* **14**, 3808-3816 (2002).
30. Lou, X. W. & Zeng, H. C. Complex α-MoO_3 nanostructures with external bonding capacity for self-assembly. *J. Am. Chem. Soc.* **125,** 2697-2704 (2003).

Supplementary Information is linked to the online version of paper at www.nature.com/nature.

Acknowledgements This work was supported by the Australian Research Council (ARC). HGY wishes to express his sincere gratitude to the National University of Singapore (NUS) where the preliminary experimental work was carried out. Authors acknowledge Dr Qiu Hong Hu for her support on statistical analysis.

Author Information Reprints and permissions is available at www.nature.com/reprints. The authors declare no competing financial interests. Correspondence and requests for materials should be addressed to G.Q.L. (maxlu@uq.edu.au) & S.Z.Q (s.qiao@uq.edu.au).

METHODS

Theoretical calculations. In each calculation, stoichiometric slab models (1×1) were employed, consisting of 9 atomic layers and a total of 9 atoms for clean (001) surface, 8 atomic layers and a total of 12 atoms for clean (101) surface. For the above (001) and (101) surfaces, each surface contains one fivefold Ti, which is terminated by X (X = H, B, C, N, O, F, Si, P, S, Cl, Br, I). All atoms were relaxed without any constraint. All calculations were carried out using density functional theory within the generalized-gradient approximation[31], with the exchange-correlation functional of Perdew-Burke-Ernzerhof[32,33]. This was implemented in the Vienna ab initio simulation package[34,35], which spans reciprocal space with a plane-wave basis, in this case up to a kinetic energy cutoff of 450 eV. We used an 11×11×11 Monkhorst-Pack k-point mesh for bulk anatase, 11×11×1 for slabs, 3×3×3 for dimmers of X for final calculations of energies. During the relaxations all structures were relaxed to an energy convergence of 10^{-4} eV (equating to a force convergence of 10^{-2} eV/Å). In the case of slabs, the vacuum space is larger than 15 Å. And for the dimmers of X, a cubic unit cell with a = b = c = 16 Å was employed. For isolated atoms (to correct the cohesive energy), a unit cell with a = 15 Å, b = 16 Å, c = 17 Å was used.

Synthesis of anatase TiO_2 SCs. Hydrochloric acid (1.5 M) was used to adjust the pH of deionized water (1.0 L) to around 2.1. Titanium tetrafluoride (TiF_4, Aldrich Chemical) was then dissolved in this solution to a concentration of 0.040 M, during which the pH value changed to 1.8[36,37]. Deionized water was then used to adjust the concentration of TiF_4 aqueous solution to a concentration of 2.67 to 5.33 mM. In a typical synthesis, the 30 mL of TiF_4 aqueous solution and 0.4 mL of hydrofluoric acid (HF, 10% w/w) were added to a Teflon-lined autoclave and a transparent mixture formed; the mixture was kept at 180 ^{o}C for 2 - 20 h in an oven. After completion of

the reaction, the clear solution at the upper section was carefully removed by a plastic dropper and a precipitate (TiO_2 product) formed at the bottom of the Teflon reactor. The solid products obtained were washed three times with deionized water (15 mL each time) and then dried at 100 ^oC or redispersed in deionized water for further characterization.

Fluorine removal from the surface of anatase TiO_2 SCs. Typically, the powder samples of as-prepared anatase TiO_2 SCs were heat-treated in static air in a Muffle furnace at temperatures of 200 to 600 ^oC for 90 min with a ramping rate of 5 ^oC/min. The samples were cooled down to room temperature in the Muffle furnace following the heat treatment for further characterization.

Materials characterization. Crystallographic information of anatase TiO_2 SCs was obtained with X-ray diffraction (XRD, Shimadzu XRD-6000, Cu Kα radiation). Chemical compositions of anatase TiO_2 SCs were analyzed with X-ray photoelectron spectroscopy (XPS, Kratos Axis ULTRA incorporating a 165 mm hemispherical electron energy analyser). All binding energies were referenced to the C1s peak (285.0 eV) arising from adventitious carbon. Prior peak deconvolution, X-ray satellites and inelastic background (Shirley-type) were subtracted for all spectra. Morphology and crystal structure of anatase TiO_2 SCs were examined with scanning electron microscopy (SEM, JEOL JSM6400F & JSM890) and transmission electron microscopy (TEM, Philips Tecnai T12 and T30F FEG Cryo AEM). Samples of anatase TiO_2 SCs were dispersed in deionized water and dropped on a conductive SEM sample holder, or a carbon-coated copper grid with irregular holes for electron microscopy (SEM/TEM) analysis. XPS and XRD samples were prepared by drying the sedimented particles overnight at 100 ^oC.

31. Kohn, W. & Sham, L. J. Self-consistent equations including exchange and correlation effects. *Phys. Rev. B* **140**, A1133 - A1138 (1965).
32. Perdew, J. P., Burke, K. & Ernzerhof, M. Generalized gradient approximation made simple. *Phys. Rev. Lett.* **77**, 3865-3868 (1996).
33. Kresse, G. & Joubert, D. From ultrasoft pseudopotentials to the projector augmented-wave method. *Phys. Rev. B* **59**, 1758-1775 (1999).
34. Kresse, G. & Furthmüller, J. Efficient iterative schemes for ab initio total-energy calculations using a plane-wave basis set. *Phys. Rev. B* **54**, 11169 - 11186 (1996).
35. Kresse, G. & Furthmüller, J. Efficiency of ab-initio total energy calculations for metals and semiconductors using a plane-wave basis set. *Comput. Mater. Sci.* **6**, 15 (1996).
36. Yang, H. G. & Zeng, H. C. Creation of intestine-like interior space for metal oxide nanostructures with a quasi reverse emulsion. *Angew. Chem. Int. Ed.* 43, 5206-5209 (2004).
37. Yang, H. G. & Zeng, H. C. Synthetic architectures of $TiO_2/H_2Ti_5O_{11}\cdot H_2O$, $ZnO/H_2Ti_5O_{11}\cdot H_2O$, $ZnO/TiO_2/H_2Ti_5O_{11}\cdot H_2O$ and ZnO/TiO_2 nanocomposites. *J. Am. Chem. Soc.* **127,** 270-278 (2005).

Figure 1 Slab models and calculated surface energies of anatase TiO_2 (001) and (101) surfaces. The optimised ratios of B/A and percentage of {001} facets (S_{001}/S) are also shown. a-b, Unrelaxed clean (001) and (101) surfaces. Ti and O are labelled as gray and red spheres, with sixfold Ti, fivefold Ti, threefold O and twofold O specified as 6c-Ti, 5c-Ti, 3c-O and 2c-O respectively. **c-d**, Unrelaxed (001) and (101) surfaces covered by adsorbate atoms X (X = H, B, C, N, O, F, Si, P, S, Cl, Br, I). **e**, Calculated surface energies of (001) and (101) covered by X. Clean surfaces are employed as reference (denoted by blue sphere and circle). **f**, Plots of the optimized ratios of B/A and percentage of {001} facets (S_{001}/S) for anatase single crystals with various adsorbate atoms X. As indicated in the inset schematic diagram, two independent length parameters A and B denote the side of the bipyramid and the side of square {001} "truncation" facets respectively. The ratio of high reactive {001} facets with respect to total surface area may therefore be described by the value of S_{001}/S or B/A (where $0 \leq B/A \leq 1$).

Figure 2 SEM images and statistical data of the size and truncation degree of anatae SCs. a, The morphology of anatase SCs synthesized with 5.33 mM titanium tetrafluoride (TiF_4) aqueous solution at 180 ^{o}C for 14 h. **b**, The size (length of A) distribution of anatase SCs in **a**. **c**, The degree of truncation (assigned as B/A) of anatase SCs in **a**. **d-f**, Control over the degree of truncation of anatase SCs was fulfilled by halving the concentration of TiF_4 and extending the reaction time to 20 h. For both the size and the degree of truncation, the relative standard deviation (RSD) of all statistical data were derived from counting more than 100 SCs for each sample. The scale bars in (**a, d**) are 1μm.

Figure 3 Crystalline phase determination. a, Bright filed TEM image of a representative anatase SC recorded along the [001] axis. **b**, Anatase single-crystalline

phase can be confirmed by the square symmetric SAED pattern. The inset is a [001] projected geometrical model of the anatase SCs. **c,** High-resolution TEM image recorded from another anatase SCs with [001] orientation. **d,** FFT filtered image recorded from the white dotted rectangular area in (**c**).

Figure 4 Confirmation of the spatial distribution of F element in anatase SCs. a, A representative XRD pattern of anatase SCs in this work, which concordances well with the calculated diffraction pattern of bulk anatase (bottom). **b**, XPS spectrum of anatase SCs showing the four characteristic peaks of titanium, oxygen, fluorine, and carbon (RI = relative intensity).

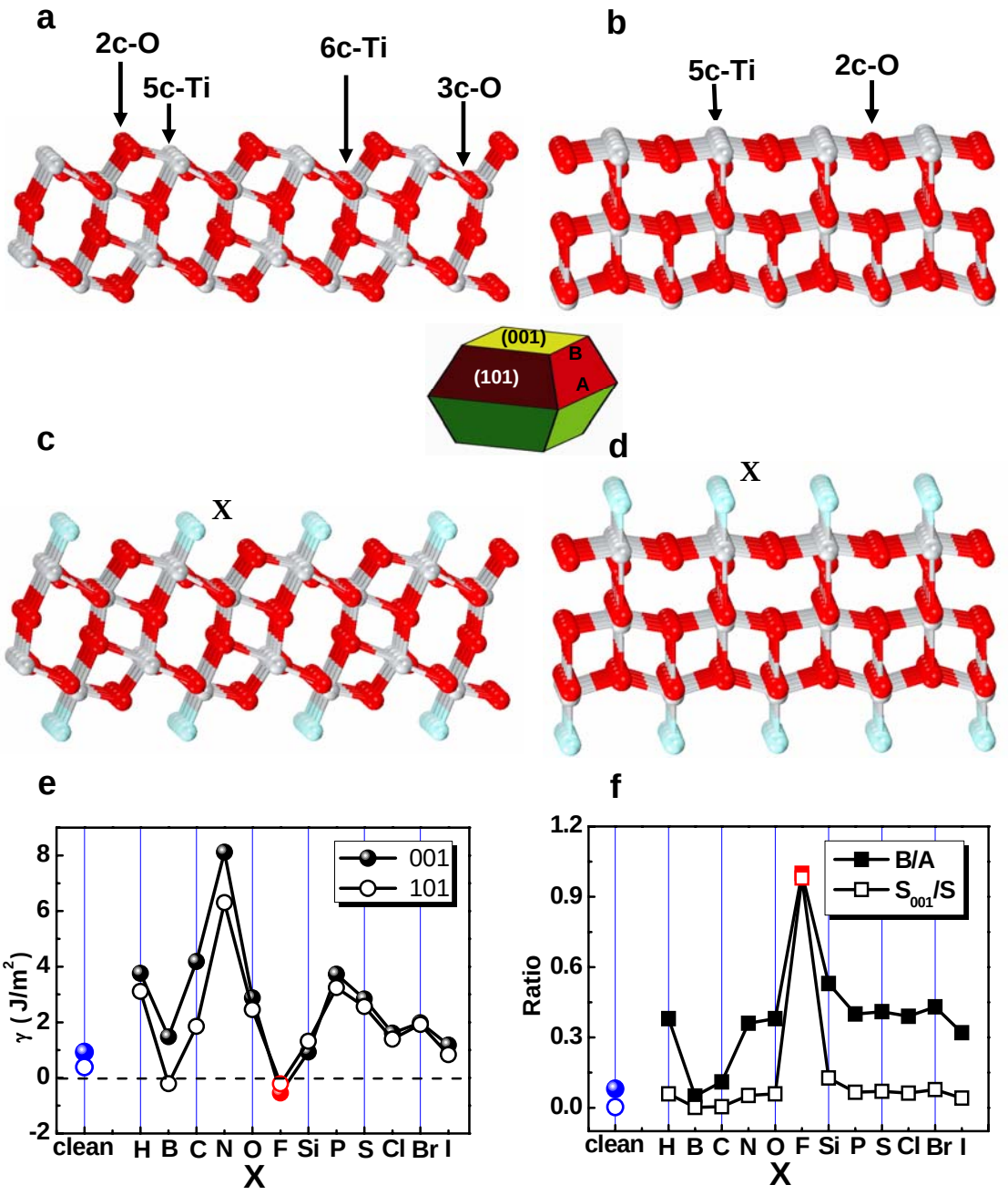
a
2c-O
5c-Ti
6c-Ti
3c-O
b
5c-Ti
2c-O
(001)
B
(101)
A
c
X
d
X
e
001
101
γ (J/m^2)
clean H B C N O F Si P S Cl Br I
X
f
B/A
S_{001}/S
Ratio
clean H B C N O F Si P S Cl Br I
X

Figure 1

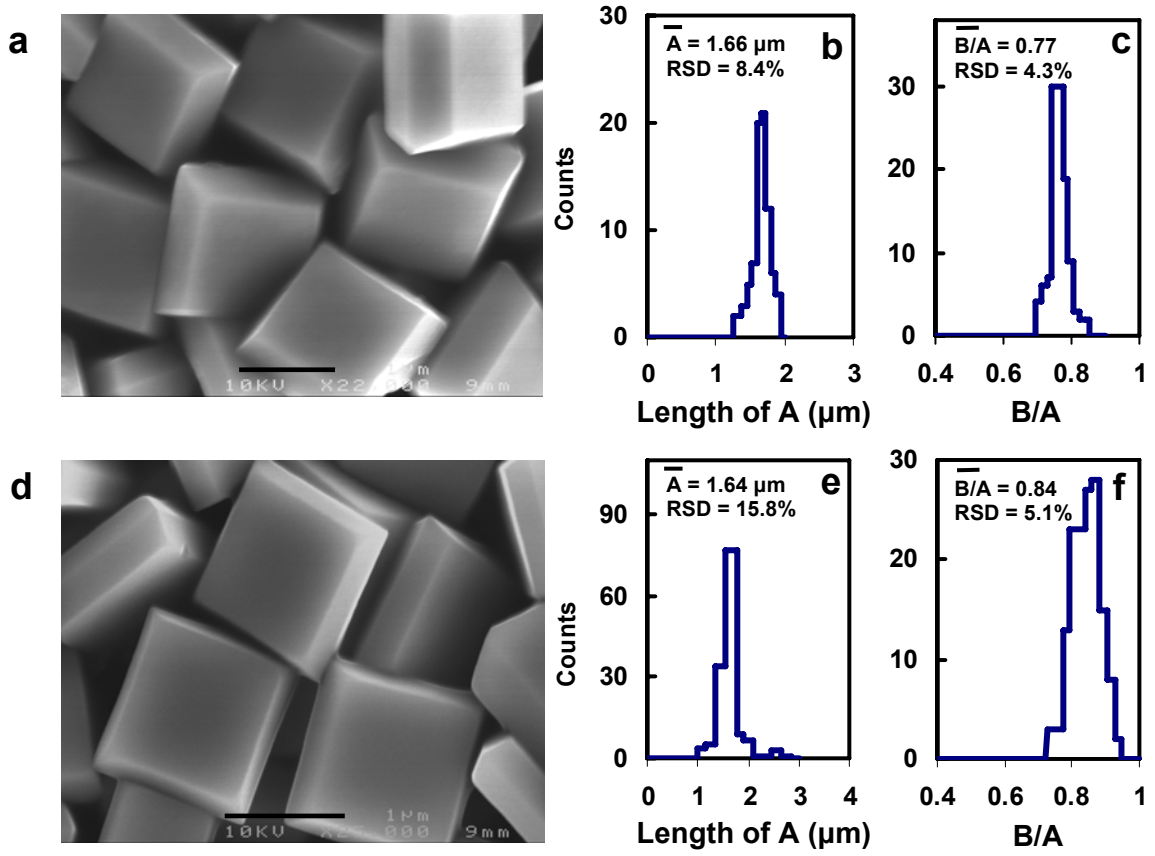
a
b
c
d
e
f
A = 1.66 µm
RSD = 8.4%
B/A = 0.77
RSD = 4.3%
A = 1.64 µm
RSD = 15.8%
B/A = 0.84
RSD = 5.1%
Counts
Length of A (µm)
B/A
10KV
1µm
9mm

Figure 2

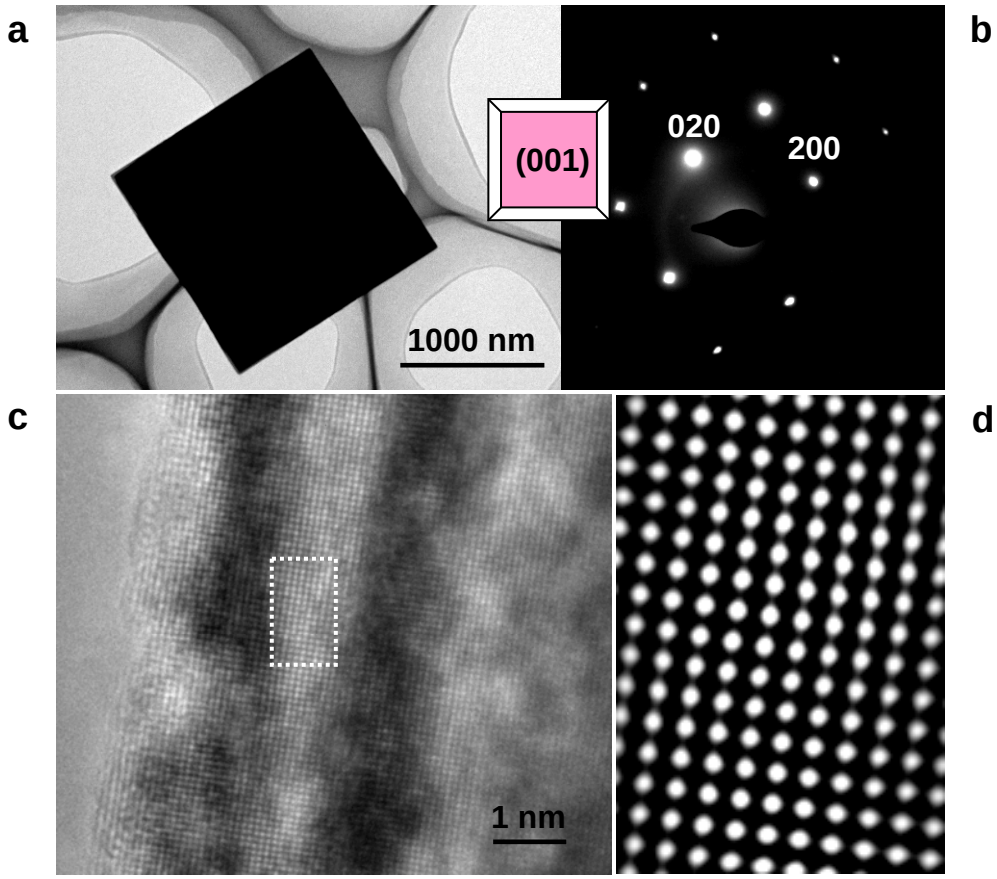

Figure 3

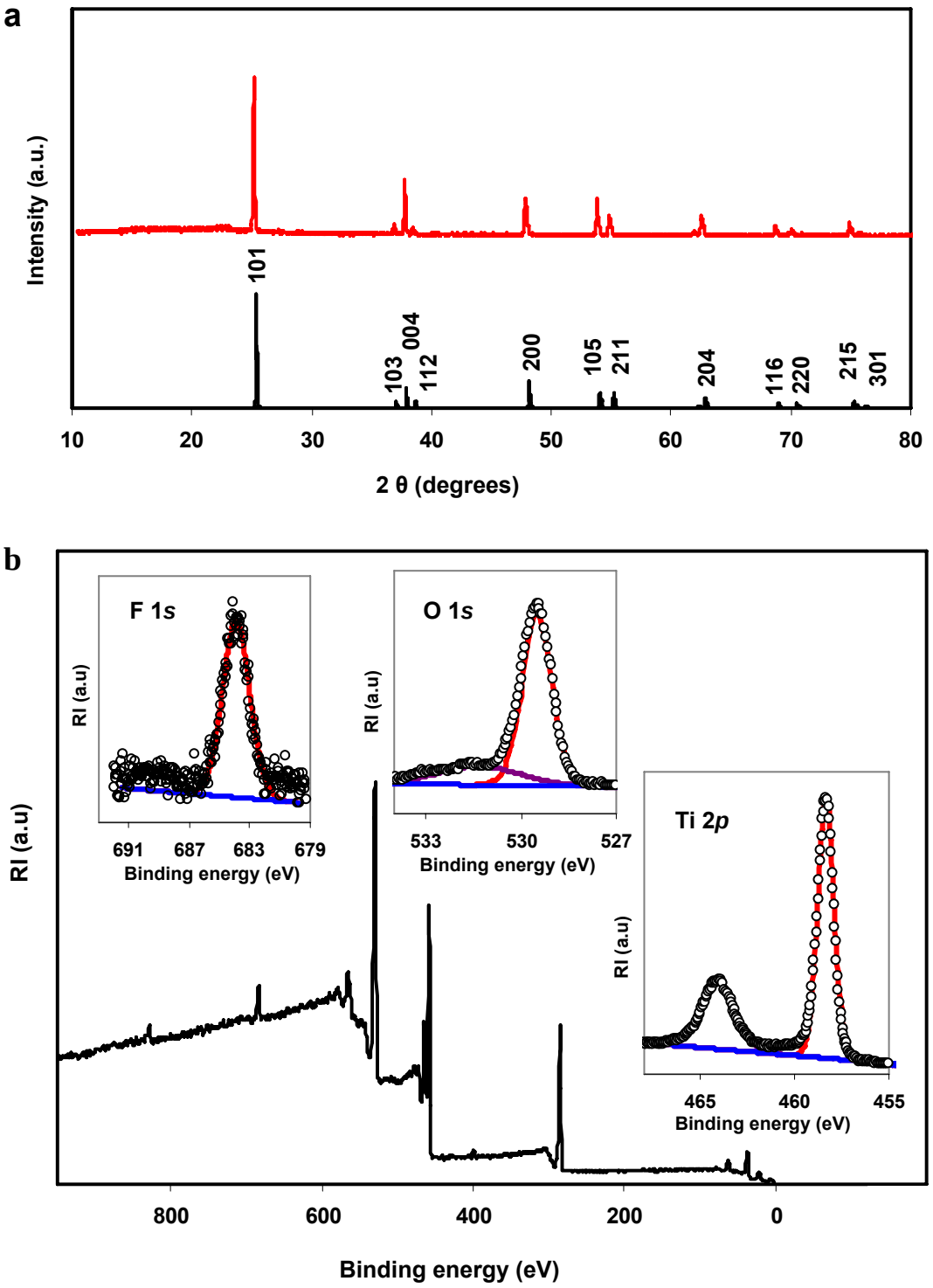
a
Intensity (a.u.)
101
103
004
112
200
105
211
204
116
220
215
301
10
20
30
40
50
60
70
80
2 θ (degrees)
b
RI (a.u)
F 1s
691
687
683
679
Binding energy (eV)
O 1s
533
530
527
Binding energy (eV)
Ti 2p
465
460
455
Binding energy (eV)
800
600
400
200
0
Binding energy (eV)

Figure 4